Caderno de Geografia (2024) v.34, n.78
ISSN 2318-2962
DOI 10.5752/p.2318-2962.2024v34n.78p.815

ORIGINAL ARTICLE

INTER-SEASONAL SPATIAL AND TEMPORAL ANALYSIS OF TRENDS AND EXTREME EVENTS IN PRECIPITATION USING GOOGLE EARTH ENGINE FOR THE XINGU WATERSHED, EAST OF THE AMAZON

Análise espacial e temporal intersazonal de tendências e eventos extremos de precipitação usando o Google Earth Engine para a bacia hidrográfica do Xingu, leste da Amazônia

Rodrigo Martins Moreira
Prof. Dr. Universidade Federal de Rondônia, Ji-Paraná-RO, Brasil
rodrigo.moreira@unir.br

Bruno César dos Santos
Pós-doutorando Universidade Federal de São Carlos, São Carlos-SP, Brasil
bcsantos@ufscar.br

Paulo Henrique de Souza
Prof. Assoc. Universidade Federal de Alfenas, Alfenas-MG, Brasil
paulohenrique.souza@unifal-mg.edu.br

Recebido: 19/06/2024
Aceito: 30/07/2024

Resumo

O regime de precipitação na bacia hidrográfica do Xingu é um aspecto importante do clima regional e tem implicações significativas para o ciclo hidrológico e a dinâmica dos ecossistemas no Bioma Amazônia. Neste artigo, apresentamos uma análise espacial e temporal da precipitação inter-sazonal. Um total de 22 estações foram selecionadas após uma verificação de consistência. Entre as análises de validação dos dados do CHIRPS com as estações pluviométricas, cerca de 52,3% apreciaram um bom desempenho do R^2 (>0,7) e uma superestimação dos menores erros durante a estação seca. Durante o período chuvoso houve redução no desempenho do R^2 (<0,7) em cerca de 71,4% das estações e com maiores erros superestimados em relação ao período seco. O CHIRPS subestima para a estação seca e superestima para a estação chuvosa. Para o período chuvoso, a tendência máxima de precipitação encontrada foi de 0,3 mm.mês-1, e a tendência mínima de precipitação encontrada foi de -0,1 mm.mês-1. Para o período seco, a tendência máxima de precipitação encontrada foi de 0,08 mm.mês-1, e a tendência mínima de precipitação encontrada foi de -0,02 mm.mês-1. Este estudo destaca a importância do sensoriamento remoto para o monitoramento da precipitação em áreas com dados limitados de pluviômetros e fornece informações valiosas para a tomada de decisões na gestão sustentável dos recursos hídricos na bacia hidrográfica do Xingu, Amazônia.

Palavras–chave: Mudanças climáticas; Desmatamento; Computação em Nuvem; Inclinação de Sen; Tendências

Caderno de Geografia (2024) v.34, n.78
ISSN 2318-2962
DOI 10.5752/p.2318-2962.2024v34n.78p.815

Abstract
The precipitation regimen in the Xingu watershed is an important aspect of the regional climate and has significant implications for the hydrological cycle and ecosystem dynamics in the Amazon Biome. This paper presents a spatial and temporal analysis of inter-seasonal precipitation. A total of 22 stations were selected after a consistency check. Among the validation analyses of the CHIRPS data with the rain gauge stations, about 52.3% appreciated a good R^2 performance (>0.7) and an overestimation of the lowest errors during the dry season. During the rainy season, there was a reduction in the R^2 performance (<0.7) in about 71.4% of the stations and with higher overestimated errors concerning the dry season. CHIRPS underestimate for the dry season and overestimate for the rainy season. For the rainy season, the maximum trend for precipitation found was 0.3 mm.month^{-1}, and the minimum trend for precipitation found was -0.1 mm.month^{-1}. For the dry season, the maximum trend for precipitation found was 0.08 mm.month^{-1}, and the minimum trend for precipitation found was -0.02 mm.month^{-1}. This study highlights the importance of remote sensing for precipitation monitoring in areas with limited rain gauge data. It provides valuable information for sustainable water resources management decision-making in the Xingu watershed, Amazon.

Keywords: Climate change, Deforestation, Cloud Computing, Sen's Slope, Trends.

1. INTRODUÇÃO

The Amazon rainforest ranks among the world's largest and most biodiverse ecosystems with dynamic and complex climate patterns. Rainfall plays a vital role in sustaining the rainforest's water cycle, which, in turn, supports its rich biodiversity. However, climate change has disrupted precipitation patterns and led to extreme weather events, posing significant risks to the ecosystems and inhabitants of the Amazon (Gatti *et al.*, 2018; Malhi *et al.*, 2018; de Medeiros; de Oliveira; Avila-Diaz, 2022).

The Xingu Basin in the Amazon region faces numerous environmental challenges that significantly impact its biodiversity and water systems. Deforestation, mining, and agriculture are major drivers of this degradation, leading to soil erosion, loss of vegetation, and water pollution. Climate change exacerbates these threats by causing variations in precipitation patterns, resulting in altered rainfall and more frequent extreme weather events such as severe droughts and floods. These climatic changes amplify the effects of deforestation, as reduced vegetation cover decreases the soil's water retention capacity, making the region more vulnerable to droughts and other climatic extremes. Furthermore, changes in precipitation can impact the basin's water resources, which are essential for local communities and ecosystems. The Xingu River, a significant Amazon tributary, supplies water to many indigenous communities and supports diverse aquatic life. Shifts in rainfall patterns can affect the river's flow and water quality, thus impacting the region's inhabitants and ecosystems (Fearnside, 2019; Siqueira *et al.*, 2021; Lucas *et al.*, 2021).

ISSN 2318-2962
DOI 10.5752/p.2318-2962.2024v34n.78p.815

Monitoring extreme precipitation is crucial for the Xingu watershed and the Amazon region. However, the current network of rain gauges in the Xingu watershed, a vital area for biodiversity, is sparse and unevenly distributed. To address the limited rainfall data, remotely sensed precipitation products are essential. These remote sensing tools provide several benefits over traditional rain gauges, such as wider spatial coverage, higher temporal resolution, and cost-effectiveness. Several remote sensing options are available for estimating precipitation, including the Tropical Rainfall Measuring Mission (TRMM), Global Precipitation Measurement (GPM), and Climate Hazards Group InfraRed Precipitation with Station data (CHIRPS) (Funk *et al.*, 2015). CHIRPS, in particular, is extensively used for monitoring precipitation and conducting climate studies due to its high accuracy, long-term data availability, and daily temporal resolution (Lucas *et al.*, 2021; de Medeiros; de Oliveira; Avila-Diaz, 2022).

In climate studies, statistical methods like the Mann-Kendall test and Sen's slope estimator extensively analyse precipitation trends in the Amazon region and globally (Zhang *et al.*, 2020; Zhang *et al.*, 2021). The spatial representation of Sen's slope is particularly valuable for water resources management, offering detailed insights into precipitation trends across specific areas (Alfieri *et al.*, 2021). These tools are crucial for quantifying and assessing trends in precipitation, enabling researchers to detect both increasing and decreasing trends. This information is vital for climate studies, water resource management, and ecosystem monitoring (Medina *et al.*, 2023). Applying the Mann-Kendall test and Sen's slope estimator underscores their significance in understanding climate dynamics and supporting decision-making processes related to environmental management.

This work innovates by calculating the magnitude trend of change in precipitation using Google Earth Engine processing power, harvesting the potential of the free-of-cost and petabytes of data cloud computing platform. This paper presents a spatial and temporal analysis of precipitation patterns in the Xingu watershed using remotely sensed data from CHIRPS. We apply statistical methods to evaluate trends in precipitation patterns and spatialise the Sen's slope to provide insights into water resources management in the region. Our study highlights the importance of remote sensing for precipitation monitoring in areas with limited rainfall data. It provides valuable information for decision-making in water resources management in the Xingu watershed.

ISSN 2318-2962
DOI 10.5752/p.2318-2962.2024v34n.78p.815

2. MATERIAL AND METHODS

2.1. Study Area

The Xingu watershed is a significant river basin in Brazil, covering a vast area in the Amazon rainforest. Diverse ecosystems, including forests, savannas, and wetlands, characterise it. This response will provide an overview of the Xingu watershed, its area, and its main economic activities based on available scientific literature. The watershed encompasses an area of approximately 521,000 square kilometres (km²) and is situated in the eastern part of the Amazon Basin (Fearnside, 2001). This region is known for its high biodiversity, hosting numerous plant and animal species found nowhere else on Earth (Fonseca *et al.*, 2019). The Xingu River, which runs through the watershed, is a major tributary of the Amazon River, contributing significant freshwater input to the Amazon Basin.

The Xingu watershed's main economic activities have historically centred around agriculture, cattle ranching, and mining. Large-scale deforestation and conversion of forest areas into agricultural land and pastures have been observed in the region (Nepstad *et al.*, 2014). The expansion of soybean cultivation has been a prominent driver of land use change in the Xingu watershed (Aguiar *et al.*, 2016). Additionally, mining activities, particularly gold mining, have negatively impacted the environment and local communities (Hollanda *et al.*, 2020).

It is worth noting that the Xingu watershed also supports indigenous communities that rely on traditional livelihoods such as fishing, hunting, and gathering. These communities play a crucial role in the preservation of cultural heritage and the sustainable management of natural resources within the watershed (Fearnside, 2005).

The Xingu Watershed exhibits a tropical climate, as indicated by the Koopen-Geiger climate classification system, as shown in Figure 1. According to studies conducted by Silva *et al.* (2019) and Machado *et al.* (2021), most of the Xingu Watershed falls under the Af climate type, which represents a hot and humid tropical climate with no dry season. This classification is consistent with the overall climate of the Amazon rainforest region, characterised by high temperatures and abundant rainfall throughout the year.

Caderno de Geografia (2024) v.34, n.78
ISSN 2318-2962
DOI 10.5752/p.2318-2962.2024v34n.78p.815

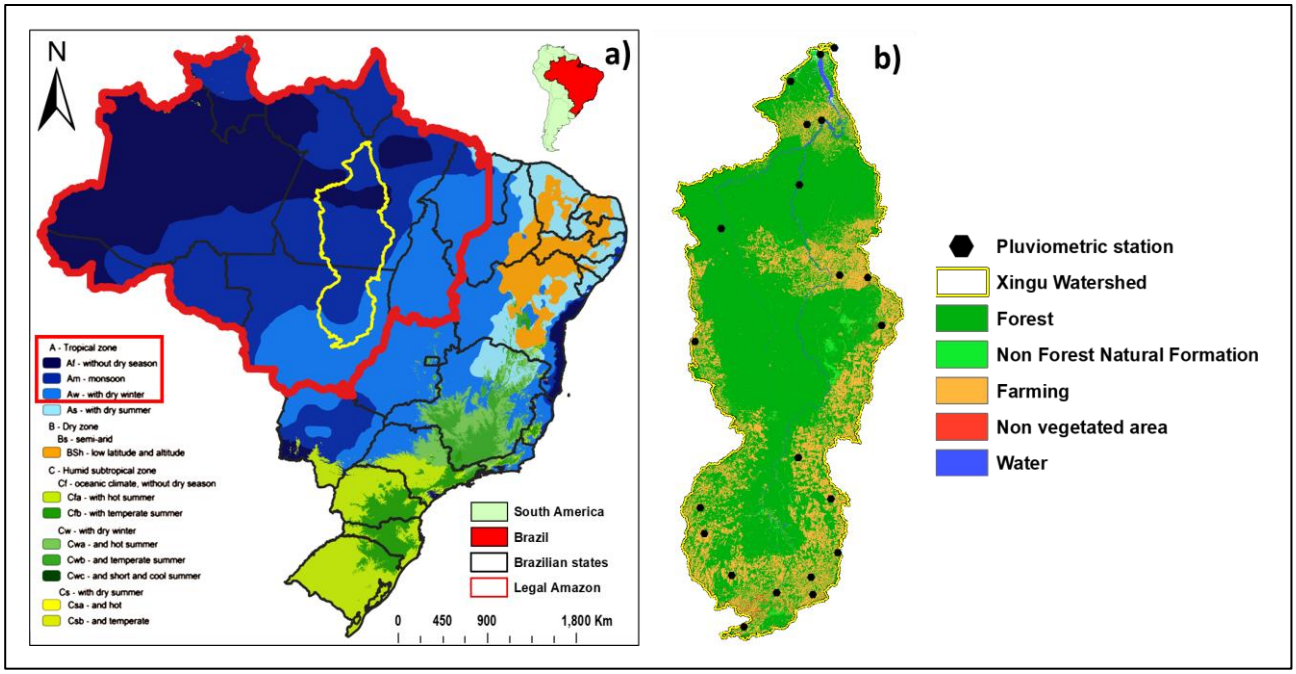

Figure 1 - Location of the study area (in yellow): a) Koppen climate classification; b) Land use and occupation and location of selected rain gauges in the Xingu river basin. **Source**: Research data.

2.2. CHIRPS precipitation data

Researchers employed classification and rainfall trend analysis tools to analyse historical precipitation data in the Xingu watershed. These methods were applied at a pixel-by-pixel level, considering monthly accumulated precipitation.

The researchers utilised the CHIRPS (Climate Hazards Group InfraRed Precipitation with Station data) dataset to obtain precipitation data. CHIRPS combines satellite-based precipitation estimates with ground-based rain gauge observations. This approach overcomes the limitations of each data source when used independently by capitalising on their respective strengths. Satellite-based estimates fill in data gaps where rain gauges are scarce or nonexistent, while rain gauges provide ground truth data to enhance the accuracy of satellite-based estimates. As a result, CHIRPS produces high-quality, high-resolution precipitation data at a resolution of 0.05°. This dataset has diverse applications, including drought monitoring and flood forecasting. The methodology employed in CHIRPS is described in detail by Funk *et al.* (2015), and its reliability has been extensively tested and validated in various regions worldwide.

The researchers obtained the CHIRPS data in matrix format and saved it as Tagged Image File (TIF) extensions. The dataset included annual precipitation values from 1981 to 2020. The process of the spatial data was deployed using Matplotlib (Hunter, 2007) and Rasterio (Gillies *et al.*, 2023) Python packages.

Caderno de Geografia (2024) v.34, n.78
ISSN 2318-2962
DOI 10.5752/p.2318-2962.2024v34n.78p.815

2.3. Metrics for Validation of CHIRPS Data

Validation analyses were performed on monthly scales. CHIRPS data was validated by superimposing the rain gauge location point over the CHIRPS image pixel. The time scale used for the tests was monthly. The coefficient of determination R2 (Equation 1) was used to validate the CHIRPS data, and the result varied between 0 and 1. The closer the value is to 1, the more accurate the representation of the values obtained by CHIRPS, with a value of 1, a perfect correlation between the data sets.

$$R^2 = \frac{\sum_{t=1}^{n}\left[\left(y_t - \underline{y}\right)\left(\hat{y}_t - \underline{\hat{y}}\right)\right]^2}{\sum_{t=1}^{n}\left[y_t - \underline{y}\right]^2 \sum_{t=1}^{n}\left[\hat{y}_t - \underline{\hat{y}}\right]^2} \qquad \text{Eq1}$$

To validate the remote sensing data, the correlation coefficient (Eq. 2) was used; the closer to 1, the better the representation of the values obtained by remote sensing, a perfect correlation between the data sets. A measure of quantification of the error associated with precipitation estimates Root Mean-Square Error (RMSE) (Eq. 2) was used.

$$RMSE = \sqrt{\frac{1}{n}\sum_{i=1}^{n}\left[Z.(x_i) - z(x)\right]^2} \quad \text{Eq2}$$

The percentage of bias (Eq. 3) represents the tendency of remote sensing values to underestimate or overestimate the values collected by the stations.

$$Pbias = \sum_{i=1}^{n} \frac{(O_i - S_i)^2}{\sum_{i=1}^{n} O_i}.100 \quad \text{Eq3}$$

Where n is the number of measured data; Oi and Si are observed and estimated data, respectively, at time *i*.

The agreement index (d) was elaborated by Willmott (1981) and used to identify the degree of agreement between the values of the stations and the values obtained by remote sensing, with 1 being a perfect agreement (Eq. 4).

$$d = \frac{\sum (o_i - e_i)^2}{\sum_{i=1}^{n} (|e_i - \underline{o}| + |o_i - \underline{o}|)^2} \quad \text{Eq4}$$

Caderno de Geografia (2024) v.34, n.78
ISSN 2318-2962
DOI 10.5752/p.2318-2962.2024v34n.78p.815

Where o is equal to the average value of the data observed by the stations and e is the remote sensing data of the CHIRPS.

Finally, the Nash-Sutcliffe efficiency coefficient was also determined. Varying from infinity to one, it states that the closer to one, the more accurate the prediction of the simulated data. The coefficient was calculated using the following formula (Eq. 5):

$$NSE = \frac{\sum (y_i - s_i)^2}{\sum (y_i - \underline{o}_i)^2}.100 \quad \text{Eq5}$$

where y_i is the observed value and $\underline{o}_i$ represents the mean of the observed value.

The Mean Squared Error (MSE) provides the mean of the squared difference between the goal value and model prediction. Following is the equation to compute the MSE value (Eq. 6):

$$MSE = \frac{1}{n}\sum_{j=1}^{n} \quad (y_i - \hat{y})^2 \qquad \text{Eq6}$$

2.4. Trend analysis - Mann-Kendall non-parametric trend test

The pixel-by-pixel analyses were performed on an annual scale to optimise the computer processing capacity. The non-parametric test of the trend for time series used in this research was proposed by (Mann, 1945; Kendall, 1975) and was applied to identify possible trends of reduction or increase of precipitation for the Xingu watershed in the time series of 39 years with data. The test is calculated according to equation 7.

$$S = \sum_{i=2}^{n} \sum_{j=1}^{i=1} signal(x_j - x_i) \text{ Eq7}$$

Where S is described as the result of the sum of (xj – xi). with xj taken as the first value after xi, n is the number of data points in the entire time series. Thus, in the peer-to-peer analysis, each pairing will be assigned the values (Eq. 8):

$$signal = \{+1 \; if \; (x_j - x_i) > 0 \; 0 \; if \; (x_j - x_i) = 0 \; -1 \; if \; (x_j - x_i) < 0 \quad \text{Eq8}$$

Caderno de Geografia (2024) v.34, n.78
ISSN 2318-2962
DOI 10.5752/p.2318-2962.2024v34n.78p.815

The probability distribution of the S statistic will tend towards normality when the number of observations (n) of the samples is large, with zero mean and variance calculated from Eq. 9:

$$VAR(S) = \frac{1}{18}\left[n(n-1)(2n+5) - \sum_{p=1}^{q} t_p(t_p-1)(2t+5)\right] \quad \text{Eq9}$$

Where tp is the amount of data with equal values in a given group, q will be the number of groups with equal values in the time series in a group p.

The Mann-Kendall test statistic is based on the value of the variable ZMK, calculated according to equation 10.

$$Z_{MK} = \{\frac{S-1}{\sqrt{VAR(S)}} \; if \; S > \; 0 \; 0 \; if \; S = 0 \; \frac{S-1}{\sqrt{VAR(S)}} \; if \; S < 0 \quad \text{Eq10}$$

2.5. Sen's Slope Analysis

Once significant trends have been identified, it is important to estimate the magnitude of this trend. For the test, the annual temporal scale was used. In the various methods applied for this purpose, the normality of the dataset is a prerequisite, being highly sensitive to outliers. To overcome this limiting factor, applying a more robust test adapted to non-parametric data, such as Sen's Slope (SS), is necessary to identify magnitudes in time series trends (Eq. 11).

$$SS = Median\left\{\left[\left(\frac{x_i - x_j}{i-j}\right)_{j=1}^{j=n-1}\right]_{i=j+1}^{i=n}\right\} \quad \text{Eq11}$$

where x_i and x_j are pairs at given times i and j ($j > i$), respectively.

3. RESULTS

Table 1 shows the percentage of failures presented in each pluviometric station along the historical series. Among the stations, the variation in percentage was at least 6.2% (00352005) and at most 28.5% (00750000). In addition, only 22% of the stations had failures below 10% of the historical series. On the other hand, about 54.5% of the stations had failures between 10% and 20%, and finally, approximately 22.7% of the stations had failures above 20% in their historical records.

ISSN 2318-2962
DOI 10.5752/p.2318-2962.2024v34n.78p.815

Table 1 - Information and faults on selected rainfall stations within the study area.

Station Code	Longitude	Latitude	Missing data (%)
01453000	-53.9986	-14.6119	8.28056845
01354000	-54.2811	-13.4483	11.5168144
01353001	-53.2417	-13.8419	14.8585901
01352001	-52.4544	-13.4956	10.2926692
01352000	-52.4128	-13.8836	12.4665822
01255002	-54.9125	-12.5178	14.0847052
01251001	-51.8264	-12.9397	8.32278036
01154001	-54.9981	-11.9292	15.0344731
01152000	-51.9889	-11.73	27.0578303
01052000	-52.7461	-10.8072	11.3198255
00855000	-55.1194	-8.1872	7.09863515
00750000	-50.8289	-7.8283	28.5211763
00651002	-51.1492	-6.7444	27.205572
00651001	-51.7986	-6.7025	21.1833404
00554000	-54.5208	-5.6503	13.1771493
00452000	-52.7203	-4.6656	11.6364148
00352005	-52.5419	-3.3078	6.24736176
00352001	-52.2131	-3.2142	15.7380048
00351002	-51.5681	-3.7231	15.8998171
00252001	-52.9186	-2.3364	11.4253553
00152001	-52.2333	-1.7333	18.0104123
00151003	-51.9178	-1.5825	23.0688054

Source: Research data.

Table 2 summarises the results of the applied metrics (RMSE, MSE, NSE, R^2, d and PBIAS) for verifying the error and correlation between the data observed on the surface and those estimated by satellite.

Among the error values, the RMSE obtained annual values ranging between 54.6 and 196.7 mm between posts. Around 86.3% of the posts show errors in millimetres below 88 mm, and only 13.2% show errors above 100 mm.

ISSN 2318-2962
DOI 10.5752/p.2318-2962.2024v34n.78p.815

Table 2 - Analysis of monthly precipitation between ground stations and satellite pixels. Variables refer to root mean square error (RMSE); Mean Squared Error (MSE); Nash-Sutcliffe efficiency coefficient (NSE); the coefficient of determination (R2); Willmott concordance index (d), and percentage of bias (PBIAS).

Rain gauge Code	RMSE	MSE	NSE	R2	d	PBIAS
151003	144.62	20916.0	0.09	0.09	0.57	7.67
152001	58.98	3479.15	0.79	0.79	0.82	-5.14
252001	66.06	4363.88	0.79	0.79	0.81	4.48
351002	111.03	12327.67	0.42	0.42	0.71	33.08
352001	81.39	6623.66	0.7	0.7	0.81	-3.97
352005	75.23	5659.33	0.78	0.78	0.8	0.96
452000	72.4	5241.86	0.63	0.63	0.75	23.01
554000	79.15	6264.61	0.57	0.57	0.73	15.61
651001	66.48	4419.28	0.71	0.71	0.77	4.01
651002	51.02	2603.18	0.79	0.79	0.8	6.61
750000	59.17	3501.03	0.77	0.77	0.79	-3.8
855000	88.4	7814.9	0.73	0.73	0.79	-9.61
1052000	68.34	4670.55	0.74	0.74	0.81	6.19
1152000	58.62	3435.98	0.8	0.8	0.82	-0.38
1154001	196.71	38696.32	0.43	0.43	0.72	-25.05
1251001	64.92	4214.91	0.77	0.77	0.82	4.55
1255002	63.8	4071.08	0.75	0.75	0.83	11.14
1352000	60.52	3662.52	0.76	0.76	0.83	10.71
1352001	57.16	3267.44	0.84	0.84	0.85	3.92
1353001	56.57	3200.58	0.79	0.79	0.84	10.09
1354000	54.6	2981.48	0.86	0.86	0.85	-3.13
1453000	61.14	3737.89	0.81	0.81	0.82	4.18

Source: Research data.

As for the PBIAS values, the results show a variation between -25.05 and 33.08 between posts. On the other hand, about 68.1% of the results showed an overestimation and 31.8% an underestimation of the error values when comparing the values of the surface stations with those of the satellite. Despite this, it is observed that only 9% of the results had error values close to zero, which is considered similar.

ISSN 2318-2962
DOI 10.5752/p.2318-2962.2024v34n.78p.815

Regarding the correlation values, the NSE showed a good relationship with values above 0.7 for about 77.2% of the stations, mainly the stations 01152000, 01352001, 01354000 and 01453000, which presented values above 0.8. On the other hand, 22.7% of the stations showed a low correlation below 0.7, mainly station 00151003, which had the worst relationship with a value of 0.

The R^2 values also showed a good correlation (>0.7) between the two compared databases in about 77.2% of the stations, mainly the stations 01152000, 01352001, 01354000 and 01453000, which had the best correlations with values above 0.8. Only 22.7% of the ranks exhibited a low correlation (<0.7), with rank 00151003 again showing the worst correlation. Finally, the “d” values show an agreement above 0.7 for about 95.4% of the posts, and only post 00151003 showed a low agreement of 0.57.

Figure 2 presents maps with the values of the applied metrics (RMSE, R^2, d and PBIAS) in a spatialised form for error verification and correlation of data observed on the surface with those estimated by satellite in the Xingu watershed.

It is noted, spatially, within the Xingu watershed, that the RMSE (Fig. 2a) error values showed errors greater than 160 mm in the western region of the basin. On the other hand, the southern portion of the basin showed smaller errors, below 100 mm, and in the rest, errors were around 140 mm. For the spatialised values of PBIAS (Fig 2d), the northern region of the basin presented higher overestimation values than the southern and western portions of the basin. Overall, the PBIAS values show a slight average overestimation of 18.7 for much of the Xingu watershed.

As for data correlation, the spatialised values of R^2 (Fig 2b) showed a better performance in the southern portion of the basin, with values above 0.6. In the rest of the basin, the R^2 values exhibited a drop in correlation below zero and, in the northern portion, with negative values, an inverse correlation concerning the southern portion.

Finally, the spatialised values of d (Fig 2c) show a better performance above 0.7 in the southern portion and a low performance (<0.5) in the northern part of the basin. Generally, most basins present low performance compared to the values (station and satellite).

Caderno de Geografia (2024) v.34, n.78
ISSN 2318-2962
DOI 10.5752/p.2318-2962.2024v34n.78p.815

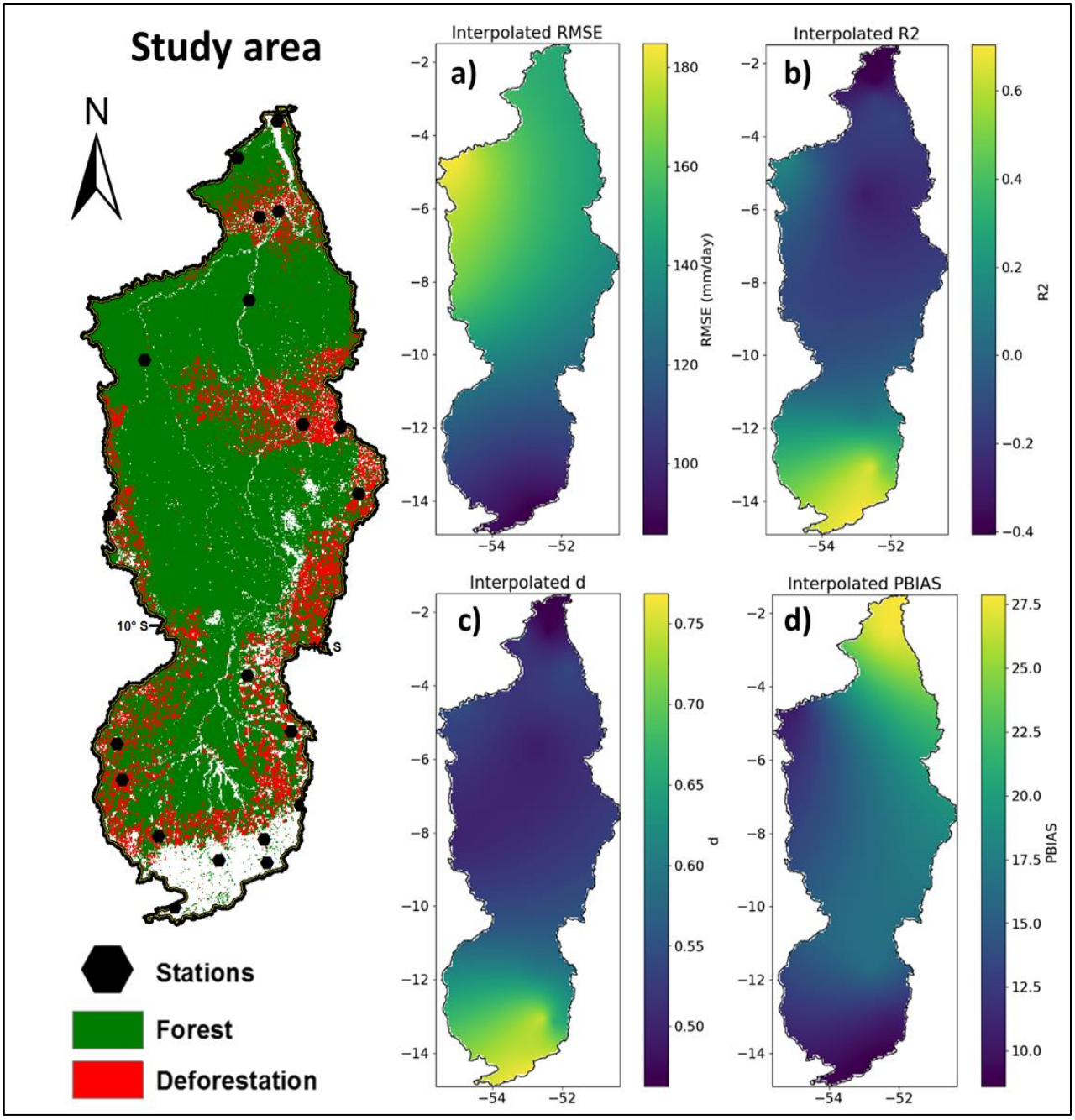

Figure 2 - Spatialised values of the applied metrics (annual): a) root mean square error (RMSE); b) determination coefficient (R2); c) Willmott concordance index (d); d) percentage of bias (PBIAS).
Source: Research data.

Table 3 summarises the precipitation trends of the stations within the Xingu basin. Among the stations, about 86.3% show that there is no change in precipitation trends. However, only 13.6% of the stations showed a trend towards reduced rainfall, as evidenced by stations 151003, 554000 and 1453000.

ISSN 2318-2962
DOI 10.5752/p.2318-2962.2024v34n.78p.815

Table 3 - Monthly Mann-Kendall (MK) precipitation trends for the selected stations.

Rain gauge Code	MK_trend	MK_pvalue	Zmk_value	MK_slope
151003	decreasing	1.31E-09	-6.0658387	-0.224
152001	no trend	0.67191414	0.42352242	0.01848739
252001	no trend	0.5593602	-0.5837921	-0.0219697
351002	no trend	0.68037617	0.41194987	0.01461318
352001	no trend	0.63382385	0.47635168	0.01735537
352005	no trend	0.81024886	0.240105	0.00847458
452000	no trend	0.84377254	-0.1970703	-0.0054945
554000	decreasing	0.00259404	-3.0121503	-0.1029488
651001	no trend	0.278928	-1.0827306	-0.0388889
651002	no trend	0.99123823	0.01098147	0
750000	no trend	0.50411274	-0.6680327	-0.0171429
855000	no trend	0.06403078	1.85196547	0.07931034
1052000	no trend	0.16624219	-1.3843798	-0.0210386
1152000	no trend	0.48482505	0.6985632	0
1154001	no trend	0.16544794	1.38697974	0
1251001	no trend	0.83310973	-0.2107149	0
1255002	no trend	0.57760081	-0.5568926	0
1352000	no trend	0.30960627	-1.0160485	0
1352001	no trend	0.56007171	-0.582735	0
1353001	no trend	0.09842693	-1.6525281	-0.0235
1354000	no trend	0.83825939	-0.2041204	0
1453000	decreasing	0.02483977	-2.2438854	-0.0458537

Source: Research data.

Note in Figure 3a that the rainfall trend over the basin shows an increasing pattern in the central-north region, except for the northern end, which showed a downward trend. On the other hand, the central-southern region of the basin showed trends of reduction in precipitation, mainly areas in the central-east, where there was a strong reduction in the volume of rainfall.

Caderno de Geografia (2024) v.34, n.78
ISSN 2318-2962
DOI 10.5752/p.2318-2962.2024v34n.78p.815

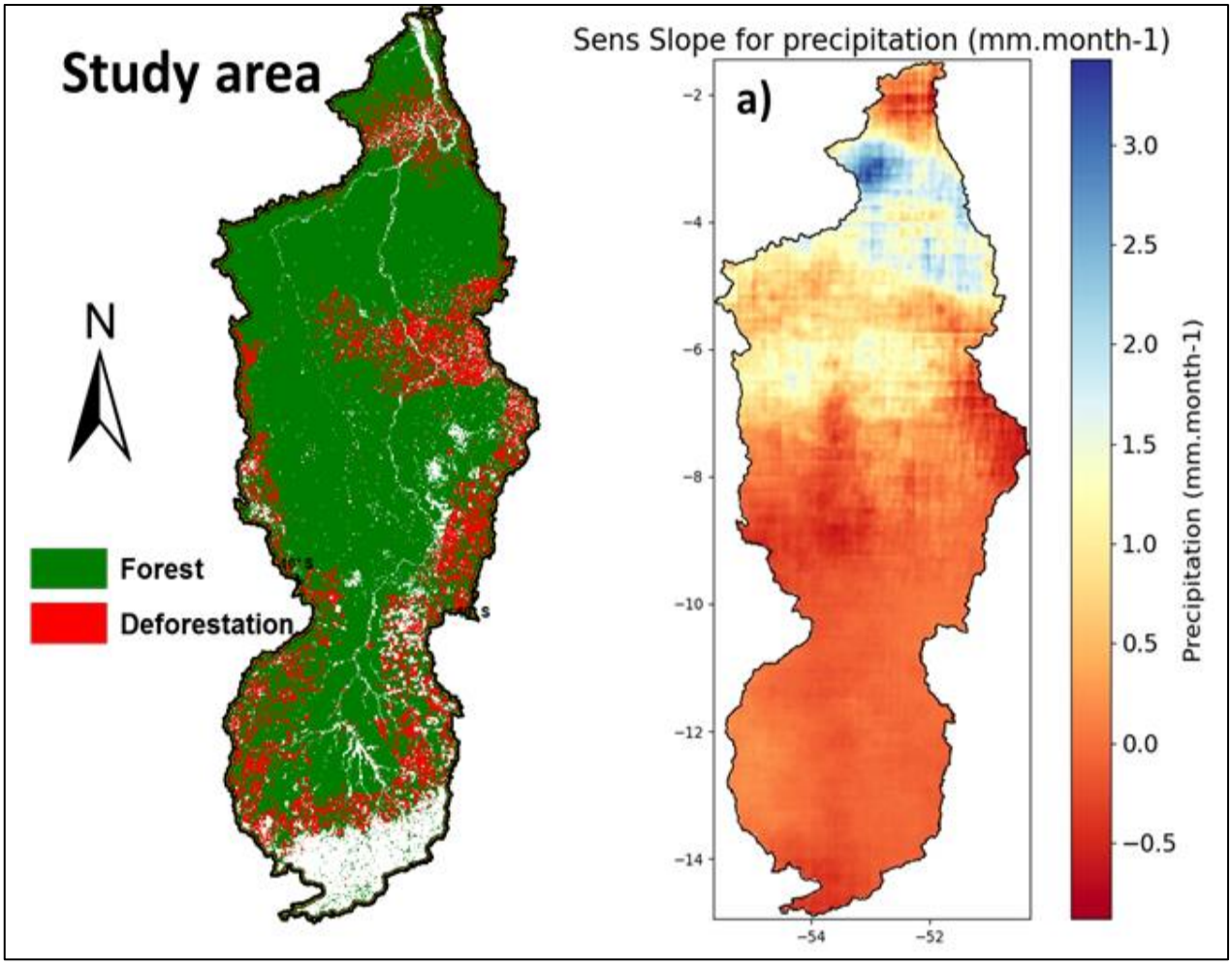

Figure 3 - Map of the rainfall trend (annual) of the applied rainfall indexes in the study area: a) Sen s Slope magnitude of the trend for precipitation value (mm.month^{-1}).
Source: Research data.

3.1. Intraseasonal analysis

Figure 4 shows the values of the metrics applied to compare the error and correlation between the values observed at surface stations and the values estimated by the satellite, separated into dry and wet periods. Among the R^2 values, about 80.9% of the stations showed good correlation with values above 0.6 for the dry period. However, about 19.1% showed correlations below 0.6, mainly rank 151003, which presented the worst performance with values close to 0. Regarding the wet period, about 71.4% of the stations had a low performance, presenting values below 0.6, mainly stations 151003 and 1154001, and only 28.5% of the stations showed a good performance, with values of R^2 above 0.6. The best correlations between the data showed a greater number of stations with better performance in the dry period than in the wet period. For d values, about 95.2% of the stations showed agreement above 0.6 for the dry period and 76.1% of the stations for the wet period. In general, the d values showed similarities with the R^2 values, where the two metrics show

Caderno de Geografia (2024) v.34, n.78
ISSN 2318-2962
DOI 10.5752/p.2318-2962.2024v34n.78p.815

better performance between surface data concerning satellite data in the dry period than in the wet period.

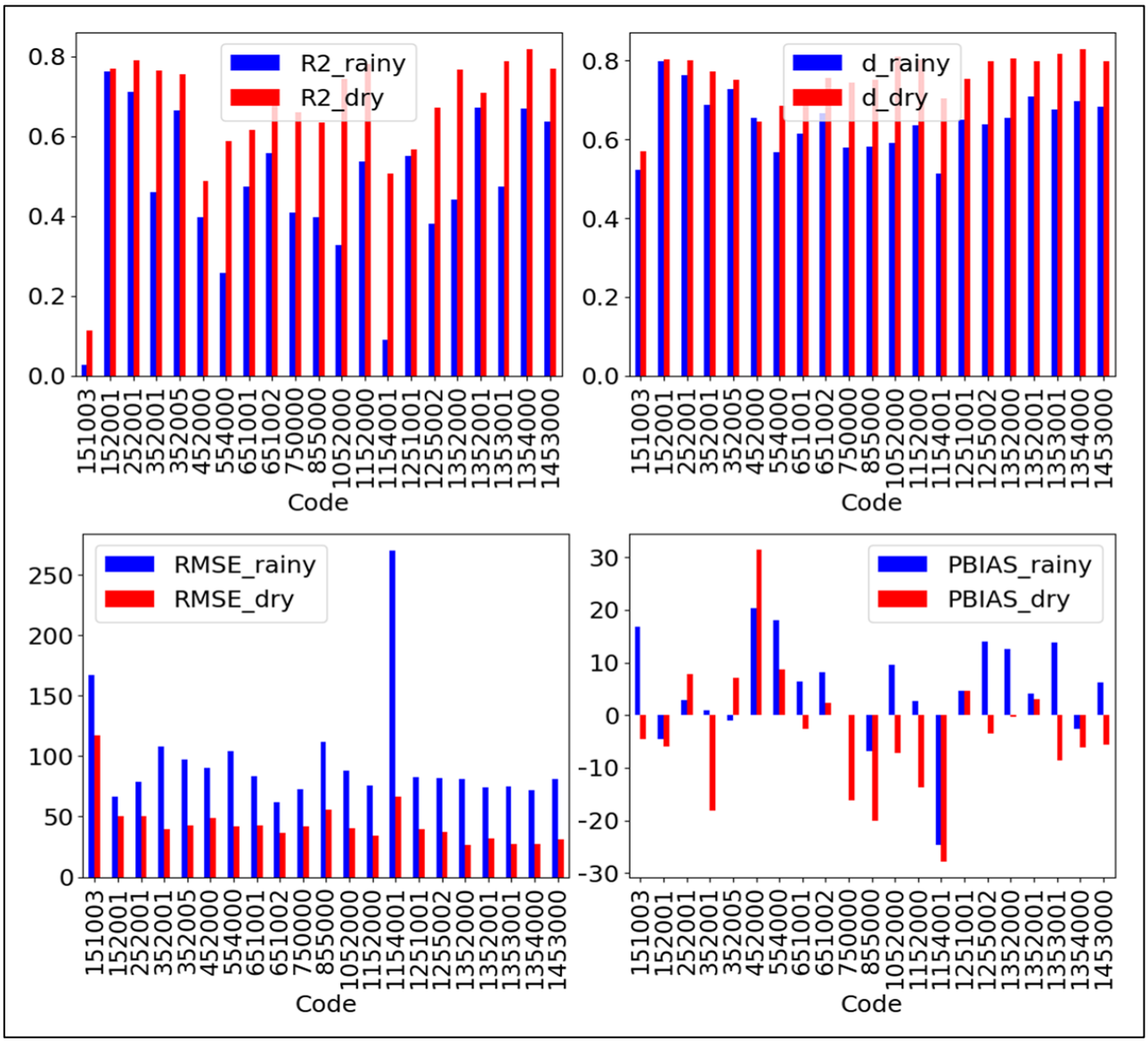

Figure 4 - Values of the applied metrics (R2, d, RMSE and PBIAS) in the selected rainfall stations, separated into rainy (blue) and dry (red) seasons. **Source**: Research data.

The RMSE values show that, in the wet period, errors are greater than 50mm for all stations, and only five of them (151003, 352001, 554000, 855000 and 1154001) showed errors above 100mm, with station 1154001 being the one that presented errors above 250mm. In the dry period, the errors were below 50mm in about 85.7% of the stations, and only 14.2% showed errors above 50mm, with station 151003 presenting errors above 100mm. In general, error values were higher during the wet period compared to the dry period. Among the PBIAS values, in the wet period, about 71.4% of the stations showed an overestimation, and approximately 28.5% presented an underestimation of the errors. In the

ISSN 2318-2962
DOI 10.5752/p.2318-2962.2024v34n.78p.815

range of PBIAS values, about 52.3% of stations had errors between 10 and -10, some very close to zero, that is, within the ideal value for PBIAS. On the other hand, about 38% of the stations had higher errors, above 10 or -10, mainly stations 452000 (overestimation) and 1154001 (underestimation), which showed the highest PBIAS errors. In the dry period, approximately 33.3% of the stations presented an overestimation and 66.6% an underestimation of the PBIAS error values. In the range of PBIAS values, about 71.4% of the stations showed errors between 10 and -10, some close to zero. On the other hand, about 28.5% of stations showed higher errors, such as station 452000 (overestimation) and station 1154001 (underestimation). In general, error values tend to be overestimated during the wet period and underestimated during the dry period.

Figure 5 shows the values of the annual precipitation trends in the wet and dry periods between seasons. It can be noted that the annual trends in precipitation showed a slight increase in about 28.5% of the stations and a slight reduction in about 42.8% of the stations. However, about 28.7% of stations showed no change in the trend in annual rainfall.

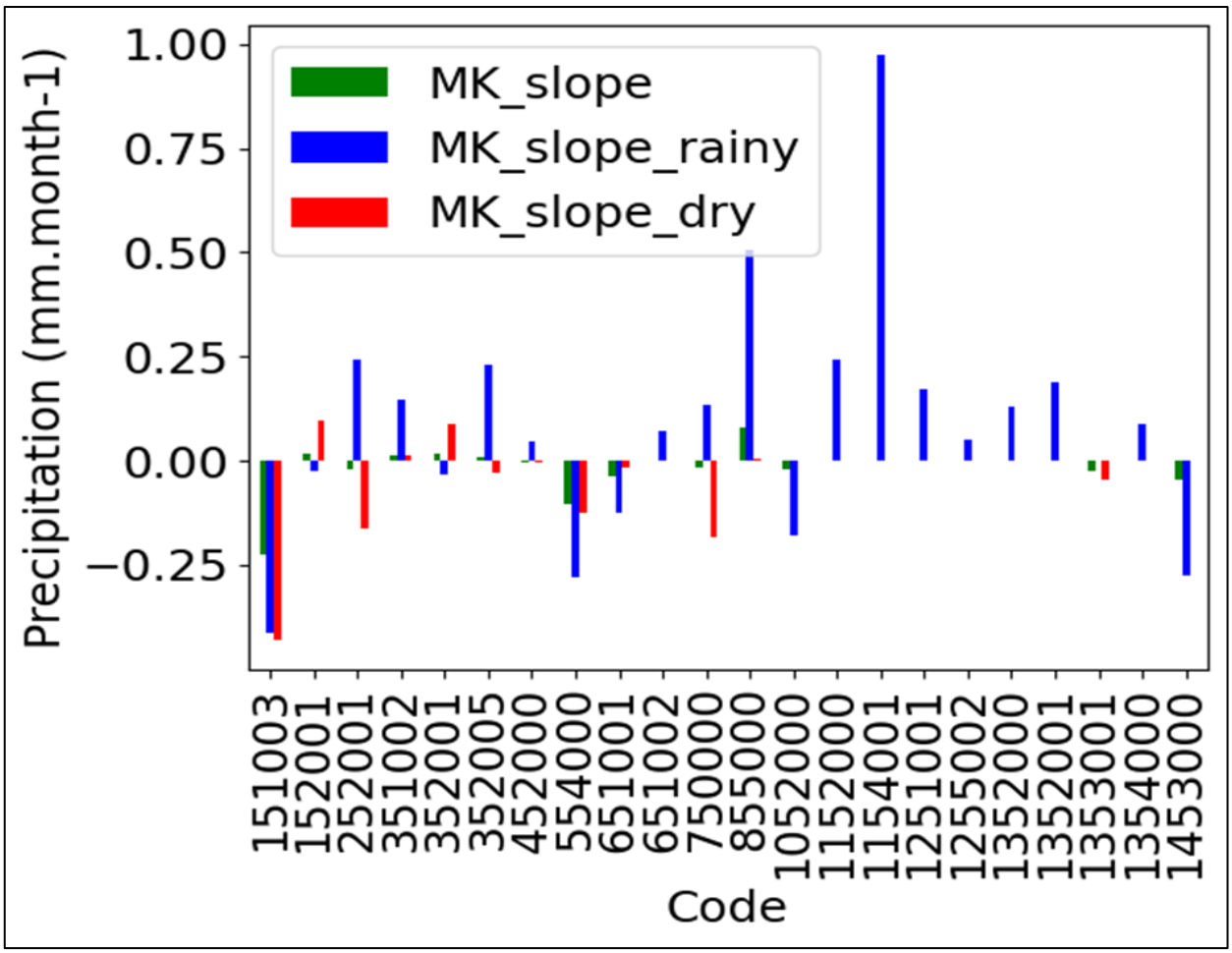

Figure 5 - Precipitation trend (Mann-Kendall slope) of the selected rainfall stations, separated into annual (green), rainy (blue) and dry (red) seasons.
Source: Research data.

ISSN 2318-2962
DOI 10.5752/p.2318-2962.2024v34n.78p.815

For the wet period, the trends showed an increase in about 66.6% of the stations, mainly in stations 855000 and 1154001, which presented higher trend values. On the other hand, only 33.3% of the stations showed trends of reduced precipitation during the wet period. In the dry period, about 19% of the stations showed a trend towards increased precipitation and about 33.3% towards a reduction, mainly station 1511003, which showed a more significant reduction. However, about 47.6% of the stations had no change in trends for the dry season. In general, rainfall trends in the three analysed periods show that, during the wet period, rainfall volumes increased between 0.2 and 1.0 mm compared to the dry period or annually.

3.2. Rainy season analysis

Table 4 summarises the results of the metrics applied for error verification (RMSE and PBIAS) and correlation (R^2 and d) between data observed on the surface and estimated by satellite for the wet period.

Among the error values, the RMSE obtained values in the wet period that varied between 62 and 270.3 mm between seasons. About 76.1% of the stations show errors in millimetres below 100 mm, and only 23.8% show errors above 100 mm during the wet season. The results show a variation between the PBIAS values -24.5 and 20.3. Among the stations, about 66.6% of the results showed an overestimation and 23.8% an underestimation of the error values, compared with the surface stations' values with the satellite ones. Despite this, it is observed that only 9.5% of the results had error values close to zero, which is considered similar.

The R^2 values also showed a moderate correlation (>0.6) between the two databases compared in about 28.5% of the stations, mainly stations 152001 and 252001, which had the best correlations with values above 0, 7. On the other hand, about 71.4% of stations exhibited a low correlation (<0.6), with stations 252001 and 1154001 not showing any correlation. Finally, the "d" values show a moderate agreement above 0.6 for about 71.4% of the stations, and about 28.5% showed a low agreement below 0.6.

Over half of the stations present low performance, which overestimates the values between the two compared databases. On the other hand, some stations presented errors that were considered low, and there was a low agreement between the values observed by the stations and those estimated by the satellite.

ISSN 2318-2962
DOI 10.5752/p.2318-2962.2024v34n.78p.815

Table 4 - Precipitation analysis between rain gauge stations and satellite pixels during the rainy period. Variables refer to root mean square error (RMSE); the coefficient of determination (R2); Willmott concordance index (d), and the percentage of bias (PBIAS).

Rain Gauge Code	RMSE rainy season (mm.month-1)	R2 rainy season	d rainy season	PBIAS rainy season %)
651002	62.0253049	0.55870188	0.66581641	8.16856711
152001	66.6891177	0.76230265	0.79793506	-4.5441857
1354000	72.2397205	0.6695934	0.69719054	-2.6170845
750000	72.4824729	0.40795862	0.57868796	0.09011111
1352001	74.4424209	0.67217515	0.70998443	4.04694981
1353001	75.1244958	0.47455354	0.67716277	13.7792872
1152000	75.3824104	0.53600711	0.63714218	2.77036432
252001	78.6243377	0.71174765	0.76223587	2.88565005
1453000	80.8531434	0.6359375	0.68306685	6.15864598
1352000	81.4410402	0.44181058	0.65479153	12.637971
1255002	82.2475397	0.38108518	0.63873197	14.0375442
1251001	82.7599641	0.54969359	0.64930361	4.53998446
651001	83.6780506	0.47421151	0.61435953	6.30456422
1052000	87.786987	0.32718903	0.5908666	9.59824098
452000	90.0778673	0.39776589	0.65584318	20.3417945
352005	97.4993052	0.66368593	0.72865879	-1.0916555
554000	103.881342	0.25787934	0.56857201	18.0219087
352001	108.275189	0.45908184	0.68693393	0.90763738
855000	112.058058	0.39713671	0.58146303	-6.8751205
151003	167.487646	0.02637277	0.52219058	16.7235557
1154001	270.347818	0.08998185	0.51444529	-24.571918

Source: Research data.

The following Figure 6 presents, in a spatialised form, maps with the values of the applied metrics (RMSE, R^2, d and PBIAS) for error verification and correlation of data observed on the surface with those estimated by satellite for the wet period in the hydrographic basin of the Xingu.

Caderno de Geografia (2024) v.34, n.78
ISSN 2318-2962
DOI 10.5752/p.2318-2962.2024v34n.78p.815

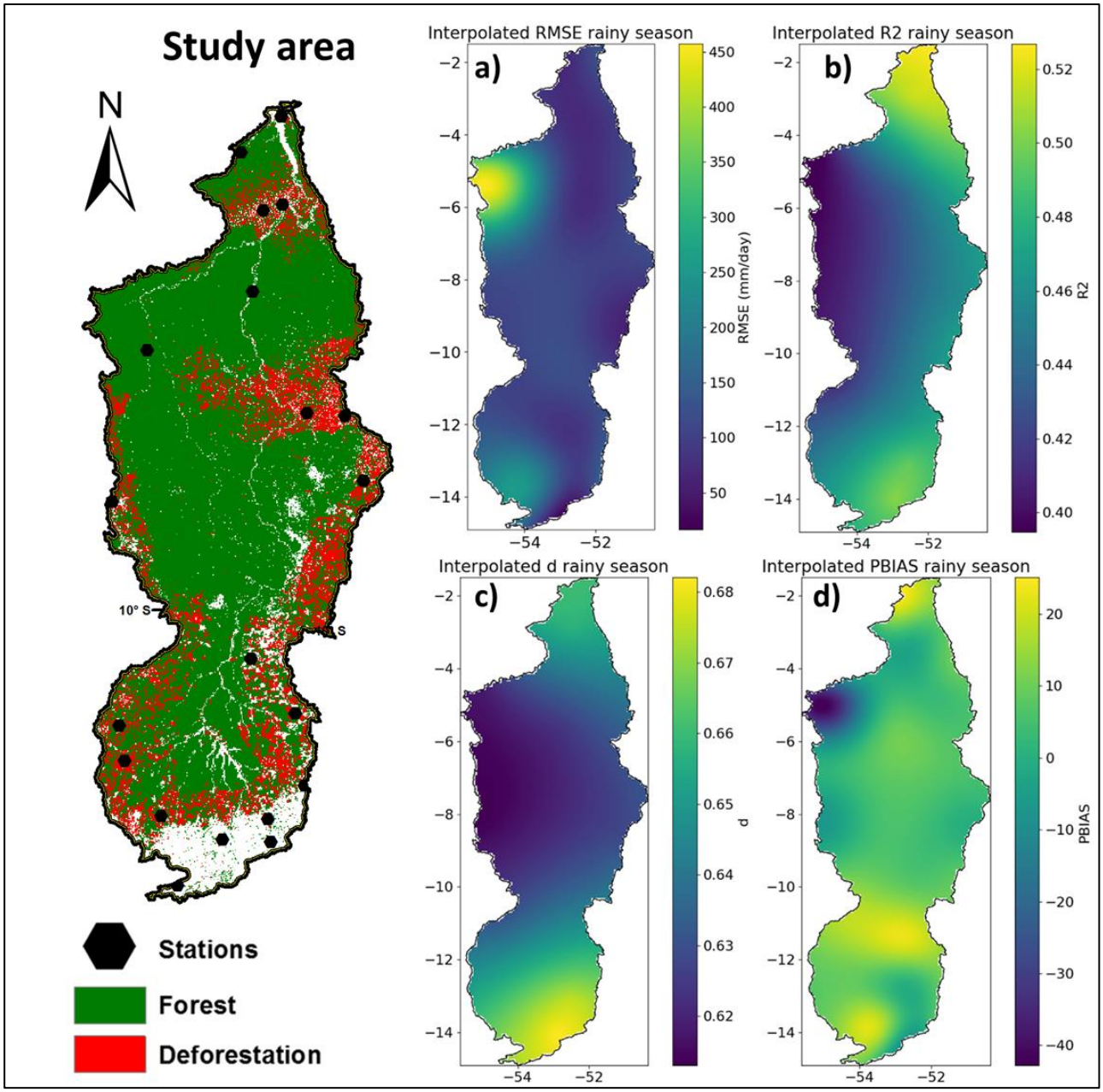

Figure 6 - Spatialised values of the applied metrics (rainy season): a) root mean square error (RMSE); b) determination coefficient (R2); c) Willmott concordance index (d); d) percentage of bias (PBIAS).
Source: Research data.

It is noted, spatially, within the Xingu watershed, that the RMSE (Fig 6a) error values showed errors greater than 300 mm in the northwest and southwest regions of the basin. On the other hand, in most of the basin, smaller errors were shown, below 100 mm, mainly in the eastern and southern portions. For the spatialised values of PBIAS (Fig 6d), the north and south regions of the basin presented high overestimation errors to the northwest portion, which had high underestimation errors. The error values were slightly closer to zero in the rest of the basin.

ISSN 2318-2962
DOI 10.5752/p.2318-2962.2024v34n.78p.815

Regarding the data correlation, the spatialised values of R^2 (Fig 6b) presented a better performance in the north and southeast portions of the basin, with values above 0.5. In the rest of the basin, the R^2 values exhibited a drop in correlation below 0.5, mainly in the western portion, where the R^2 values were 0.4.

Finally, the spatialised values of d (Fig 6c) show a better performance in the southern portion, with a value of 0.68, and a poor performance of 0.62 in the western part of the basin.

Most of the basin generally has low error and performance values compared to the databases (station and satellite).

Table 5 summarises the wet season precipitation trend values between stations within the Xingu basin. Between seasons, about 72.7% show no change in precipitation trends. However, around 13.6% of the stations showed a decreasing trend, as evidenced by stations 151003, 554000 and 1453000, and 13.6% of increased rainfall, as evidenced by stations 855000, 1152000 and 1154001, for the wet season, in the Xingu basin.

Table 5 - Mann-Kendall (MK) precipitation trends for the rainy season for the selected stations.

Rain Gauge Code	MK trend rainy season	MK p-value rainy season	Zmk values rainy season	MK slope rainy season
151003	decreasing	0.00218428	-3.06396	-0.4146973
152001	no trend	0.86843832	-0.1656425	-0.0245858
252001	no trend	0.09695604	1.65979332	0.24407183
351002	no trend	0.29946686	1.03757737	0.14826683
352001	no trend	0.80280034	-0.2497246	-0.0345786
352005	no trend	0.15434356	1.42435561	0.22885122
452000	no trend	0.70203512	0.38257472	0.04573228
554000	decreasing	0.0149254	-2.4341842	-0.2795554
651001	no trend	0.23546357	-1.186402	-0.1236208
651002	no trend	0.41858813	0.80887312	0.06965772
750000	no trend	0.11548282	1.57402003	0.13348768
855000	increasing	0.00017037	3.75933363	0.50552168
1052000	no trend	0.07156332	-1.8018862	-0.1782032
1152000	increasing	0.01749258	2.37618725	0.24338349
1154001	increasing	9.20E-07	4.90792988	0.97513804
1251001	no trend	0.14437988	1.4596733	0.17212833

Continua...

Continuação...

1255002	no trend	0.57491363	0.56082971	0.0521334
1352000	no trend	0.19219358	1.30411733	0.13135558
1352001	no trend	0.09345566	1.67744418	0.18974284
1353001	no trend	0.99127872	-0.0109307	-0.0009307
1354000	no trend	0.45679651	0.74413218	0.09015798
1453000	decreasing	0.02801483	-2.1970787	-0.274728

Source: Research data.

The maps in Figure 7 show the daily rainfall trend during the rainy season in the Xingu basin using Slope Sen.

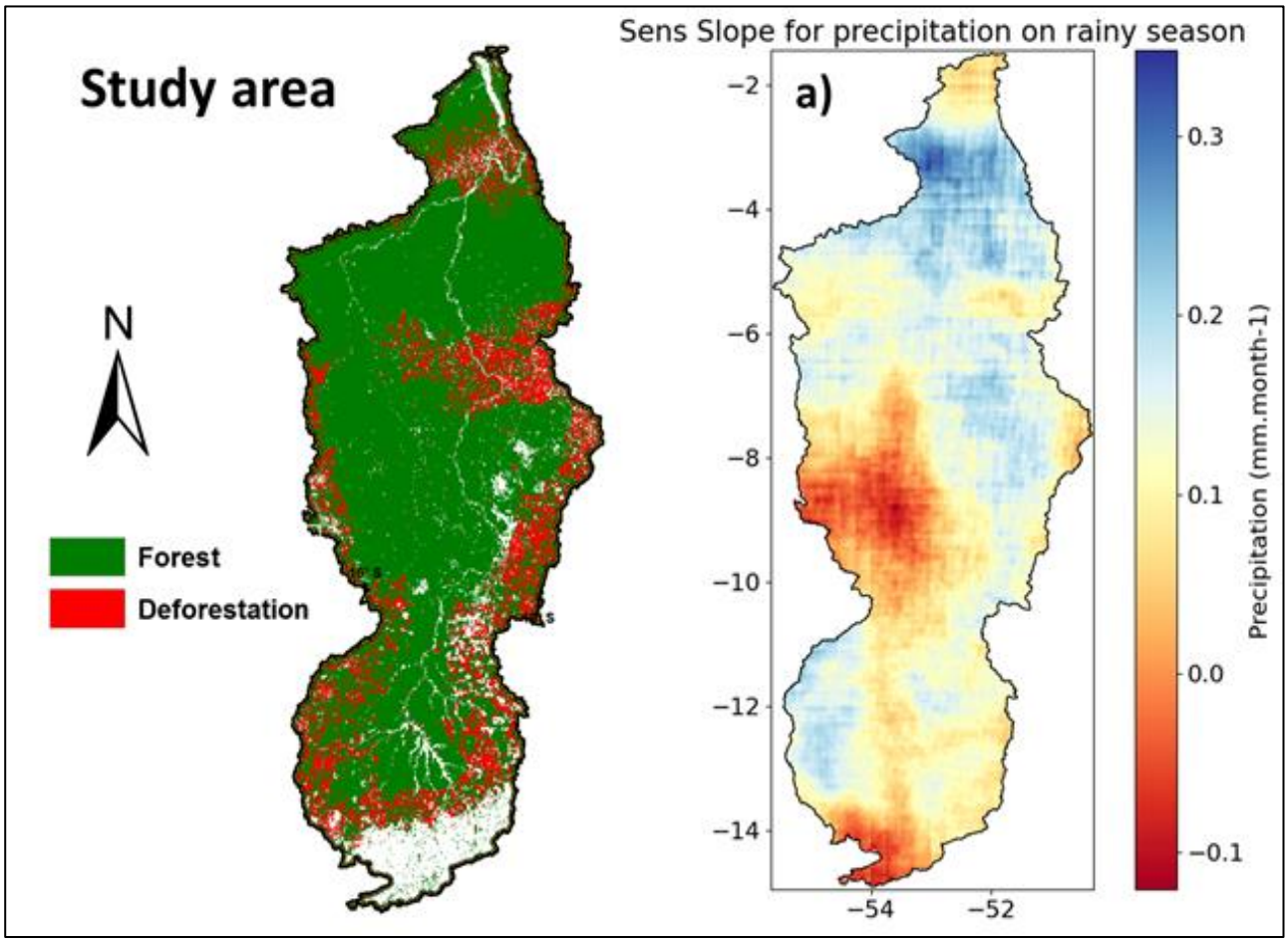

Figure 7 - Map of the rainfall trend (rainy season) of the applied rainfall indexes in the study area: a) Precipitation value (mm). **Source**: Research data.

Note in Figure 7a that the rainfall trend over the basin shows a slight pattern of increased rainfall in the north, east and southwest regions. On the other hand, the central-west and south regions of the basin showed slightly decreasing trends in rainfall volumes

ISSN 2318-2962
DOI 10.5752/p.2318-2962.2024v34n.78p.815

over these areas. Generally, most of the Xingu basin shows a pattern of increasing rather than decreasing rainfall during the wet period.

3.3. Dry season analysis

Table 6 summarises the metrics results used to analyse the errors (RMSE and PBIAS) and the correlation (R^2 and d) between the data observed on the surface and the data estimated by satellite during the dry period.

Regarding the errors, the RMSE registered values varying between 26.5 and 117.5 mm during the rainy season in the analysed stations. About 95.2% of the stations had errors below 70 mm, while only 4.7% exceeded 100 mm during the dry period. As for the PBIAS, the results ranged from -27.7 to 31.4. Among the stations, approximately 61.9% of the results indicated an overestimation. In comparison, 33.3% underestimated the errors when comparing the values of the surface stations concerning the values estimated by the satellites. However, only 4.7% of the results approached zero, indicating similar values.

The R^2 values also showed a good correlation (>0.7) in about 52.3% of the stations analysed, emphasising station 1354000, which obtained the best correlation with a value of 0.8. On the other hand, approximately 47.7% of stations showed a low correlation (<0.7), with station 1154003 registering the worst correlation, with an R^2 value of 0.1. Finally, the “d” values demonstrated a moderate agreement above 0.7 in approximately 85.7% of the stations, while approximately 14.2% presented a low agreement below this limit.

In summary, more than half of the stations showed satisfactory performance and a tendency to overestimate the values compared to the satellite databases. On the other hand, only one station presented errors that were considered high, and there was a low agreement between the values observed in the stations and the values estimated by the satellite.

It is possible to observe that, within the Xingu basin, the RMSE (Fig 8a) error values indicate errors above 50 mm in the southern region. On the other hand, in most of the basin, the errors were smaller, below 50 mm, mainly in the northern part, where the lowest errors were recorded during the dry period. As for the spatialised values of the PBIAS (Fig 8d), the southern region of the basin presented small overestimation errors compared to the western portion, which had the largest underestimation errors. In the rest of the basin, the errors were slightly underestimated.

Regarding the data correlation, the spatialised values of R^2 (Fig 8b) showed a better performance in the north and southeast parts of the basin, with values above 0.7. In the rest

ISSN 2318-2962
DOI 10.5752/p.2318-2962.2024v34n.78p.815

of the basin, there was a decrease in correlation, falling below 0.7, especially in an isolated region further south, where R^2 values were 0.6. Finally, the spatialised values of d (Fig 8c) performed well throughout the basin, with values above 0.7, especially in the northern part, where the value was 0.8 during the dry period. Most of the basin generally has low error values and good agreement between compared data from stations and satellites during the dry period.

Table 6 - Precipitation analysis between ground stations and satellite pixels during the dry period. Variables refer to root mean square error (RMSE); the coefficient of determination (R2); Willmott concordance index (d), and the percentage of bias (PBIAS).

Rain Gauge Code	RMSE dry season (mm.month-1)	R2 dry season	d dry season	PBIAS dry season (%)
651002	36.9397058	0.7140643	0.75621309	2.36408407
152001	50.149729	0.77034468	0.80399932	-6.0279846
1354000	27.4581863	0.8193738	0.83038905	-6.0555736
750000	41.9027021	0.6590636	0.74478714	-16.268051
1352001	31.6689638	0.70958674	0.79813462	3.12179438
1353001	27.7112471	0.78924048	0.81651239	-8.6271067
1152000	34.6273349	0.78127074	0.80287252	-13.662858
252001	50.5345293	0.79152767	0.80188145	7.85247719
1453000	30.8302332	0.76856302	0.79854857	-5.5610426
1352000	26.553437	0.7669248	0.80474449	-0.2408813
1255002	37.2693793	0.67254692	0.79872449	-3.5291019
1251001	39.8982137	0.56713579	0.75451505	4.59991808
651001	42.9834787	0.61652419	0.72107447	-2.6287063
1052000	40.5896159	0.74496664	0.81008513	-7.267063
452000	48.8054744	0.48757872	0.64441919	31.470683
352005	42.7666795	0.7545311	0.75043381	7.07635129
554000	41.9194301	0.58824815	0.68464054	8.62733183
352001	39.314019	0.76563869	0.77320204	-18.187055
855000	55.6153422	0.63478299	0.75129301	-20.150829
151003	117.517576	0.11234122	0.56899655	-4.5923196
1154001	66.7208083	0.50672563	0.7039223	-27.795186

Source: Research data.

Caderno de Geografia (2024) v.34, n.78
ISSN 2318-2962
DOI 10.5752/p.2318-2962.2024v34n.78p.815

The image illustrates maps that represent in Figure 8, in a spatial way, the metrics used (RMSE, R², d and PBIAS) to evaluate the precision and the correlation between the data observed on the surface and the data estimated by satellite during the dry period in the hydrographic basin of the Xingu.

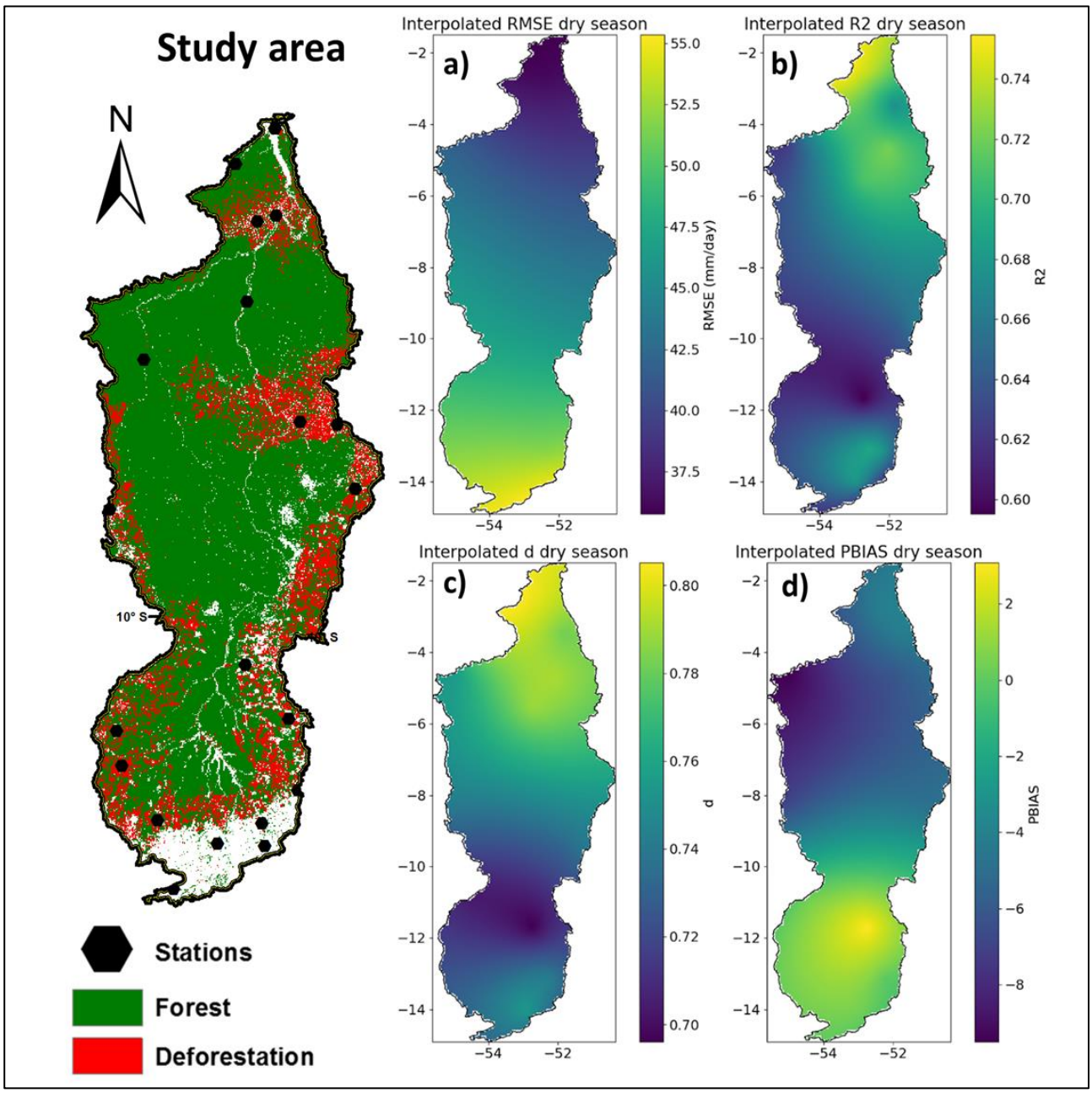

Figure 8 - Maps with the spatialised values of the applied metrics (dry season): a) root mean square error (RMSE); b) determination coefficient (R2); c) Willmott concordance index (d); d) percentage of bias (PBIAS). **Source**: Research data.

Table 7 below summarises the dry season precipitation trend values between stations within the Xingu basin. Between seasons, about 63.6% show no change in precipitation trends, and about 36.3% show a decreasing trend for the dry period in the Xingu basin.

ISSN 2318-2962
DOI 10.5752/p.2318-2962.2024v34n.78p.815

Thus, the rainfall pattern during the dry period is maintained in most stations. However, some show a reduction pattern, which may prolong the dry period in these places within the Xingu watershed.

Table 7 - Trend of dry season precipitation through Mann-Kendall (MK) between selected stations.

Rain Gauge Code	MK trend dry season	MK p-value dry season	Zmk value dry season	MK slope dry season
151003	decreasing	7.97E-08	-5.3677686	-0.4292273
152001	no trend	0.2963409	1.04431235	0.09619373
252001	decreasing	0.01163345	-2.5230721	-0.1636364
351002	no trend	0.80726493	0.24395596	0.0116489
352001	no trend	0.09180732	1.6859402	0.08733322
352005	no trend	0.63273578	-0.4778798	-0.0269565
452000	no trend	0.93474654	-0.0818745	-0.0026742
554000	decreasing	0.01349444	-2.4704468	-0.1248677
651001	no trend	0.72500718	-0.3517748	-0.0154833
651002	no trend	0.94670915	-0.0668399	-0.0009804
750000	decreasing	0.0015082	-3.1731005	-0.184
855000	no trend	0.25896815	1.12883332	0.00652174
1052000	no trend	0.68502983	-0.4056091	0
1152000	no trend	0.83817641	-0.2042266	0
1154001	no trend	0.06194381	-1.8666978	0
1251001	no trend	0.1931735	-1.3012482	0
1255002	no trend	0.20191317	-1.2761198	0
1352000	decreasing	0.00130431	-3.2150305	0
1352001	decreasing	0.0067456	-2.709149	0
1353001	decreasing	0.00031618	-3.6016681	-0.044
1354000	no trend	0.62290514	-0.4917372	0
1453000	decreasing	0.03533468	-2.104502	0

Source: Research data.

The maps in Figure 9 show the daily trend of rainfall during the dry period in the Xingu basin using the Sen's Slope.

Caderno de Geografia (2024) v.34, n.78
ISSN 2318-2962
DOI 10.5752/p.2318-2962.2024v34n.78p.815

Note in Figure 9a that the rainfall trend over the basin shows a slight increase in rainfall in the northern portion of the basin. On the other hand, the eastern portion showed trends with a slight pattern of reduction in rainfall volumes over this area. Most of the Xingu basin generally shows a trend pattern within the usual rainfall pattern during the dry period.'

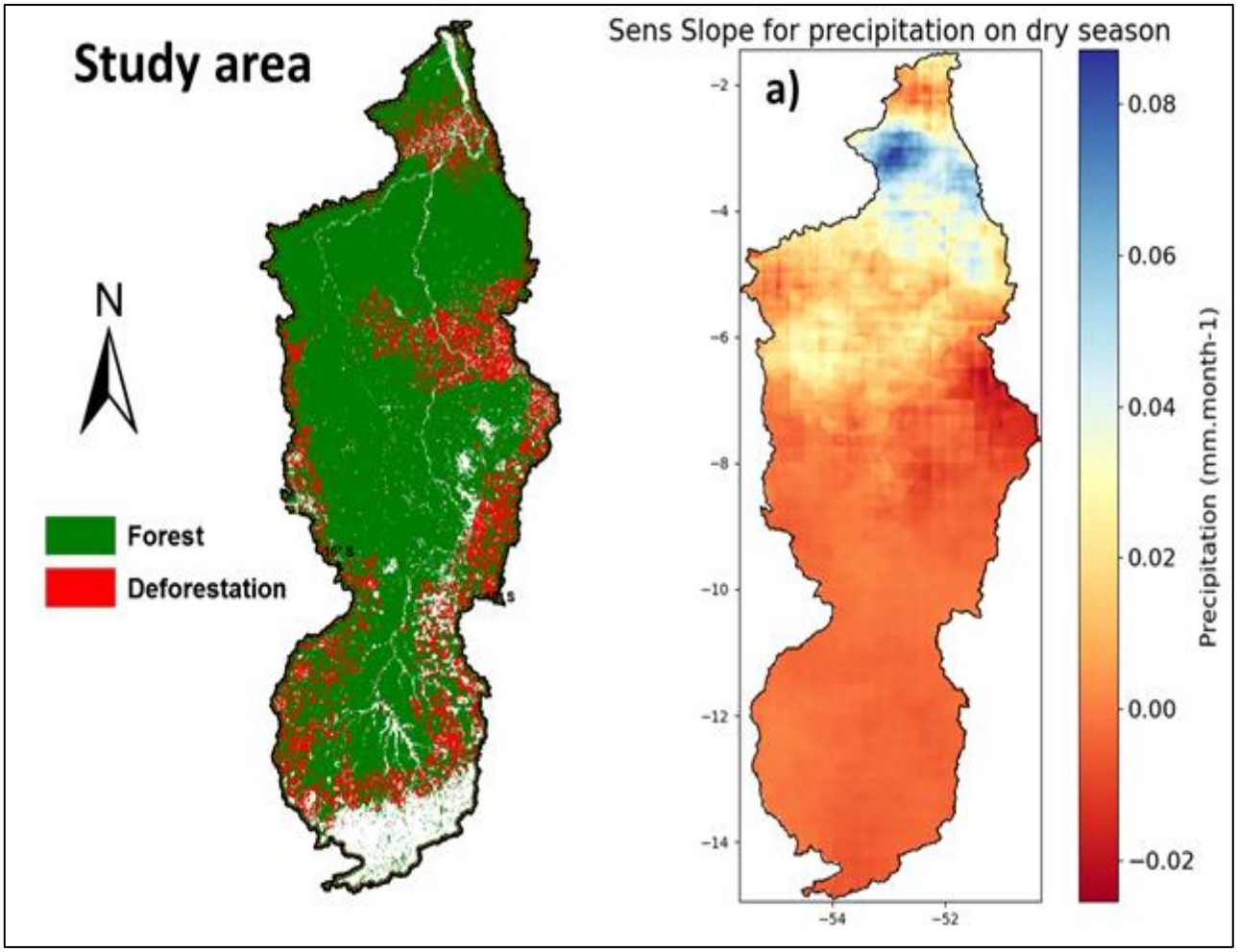

Figure 9 - Map of the rainfall trend (dry season) of the applied rainfall indexes in the study area: a) Magnitude of change - Precipitation value (mm). **Source**: Research data.

The Sen's slope analysis for the dry season reveals distinct regional variations. The northern part of the watershed shows increased precipitation, suggesting a trend towards wetter conditions in this area. The central and southern regions exhibit a decrease in rainfall, with the centre-east region experiencing the most significant decline. This prominent decrease in the centre-east is particularly concerning, as it can exacerbate existing environmental challenges, such as soil erosion and reduced water availability, further impacting the local biodiversity and water resources critical to the region. These findings highlight the importance of targeted water management strategies to address the varying precipitation trends across the Xingu watershed.

ISSN 2318-2962
DOI 10.5752/p.2318-2962.2024v34n.78p.815

4. CONCLUSIONS

Among the validation analyses of the CHIRPS data with the rain gauge stations, about 52.3% appreciated a good R^2 performance (>0.7) and an overestimation of the lowest errors during the dry season. During the rainy season, there was a reduction in the R^2 performance (<0.7) in about 71.4% of the stations and with higher overestimated errors about the dry season. Spatially, the northern portion of the basin showed better performance and lower errors in both periods (dry and wet). On the other hand, the western and central-southern portions showed a decrease in performance and higher errors in the regions of the study area.

For the trends of rainfall in the Xingu basin, some changes were observed in the rainfall regime (millimetres and number of days) during the rainy and dry seasons. About 72.7% appreciated neutrality among the stations used, and 13.6% increased or decreased rainfall during the rainy season. On the other hand, the trends during the dry period appreciated about 63.6% of neutrality and 36.3% of rainfall reduction.

REFERÊNCIAS

ALVES, D. S.; L., Shimabukuro, Y. E.; ARAGÃO, L. E. O. C. Effects of deforestation on the precipitation regime in the Xingu watershed. **Remote Sensing**, v.15, n.2, 2023.

ASSIS, T. S. MARENGO, J. A.; AMBRIZZI, T. Orography and the climatology of heavy rainfall events in the Xingu watershed. **International Journal of Climatology**, v.42, n.2, E2021-E2036, 2022.

ALFIERI, L.; PEKEL, J. F. N. J.; CARMONA-MORENO BAUMANN, F. The potential of spatially explicit trend analysis of remotely sensed time series for water resources management. **Water Resources Research**, v.57, e2020WR029238, 2021.

ALMEIDA, D. K.; BEZERRA, B. G.; RODRIGUES, S. C. Trend analysis of rainfall in the Brazilian Amazon using the Mann-Kendall and Sen's slope tests. **Environmental Earth Sciences**,v.80, n.10, p.366, 2021.

ALVES, D. S. L.; SHIMABUKURO, Y. E.; ARAGÃO, L. E. O. C. Impacts of deforestation on albedo and surface temperature in the Xingu watershed. **Remote Sensing**, v.14, n.4, p.624, 2022.

ARAÚJO, L. C.; SILVA, W. L.; & COSTA, G. N. Spatial and temporal analysis of rainfall trends in the Amazonas State, Brazil. **Atmospheric Research**, v.239, 104954, 2020.

ISSN 2318-2962
DOI 10.5752/p.2318-2962.2024v34n.78p.815

ASNER, G. P.; KNAPP, D. E.; MARTIN, R. E.; TUPAYACHI, R.; ANDERSON, C. B.; CARRANZA-JIMENEZ, L.; YEPEZ, E. A. Biodiversity and ecosystem services under siege from a global network of deforestation fronts. **Nature Ecology & Evolution**, v.4, n.3, 404-408, 2020.

ASSIS, T. S.; MARENGO, J. A.; AMBRIZZI, T. Precipitation trends in the Xingu watershed: Implications for water resources and ecosystem dynamics. **Water Resources Research**, v.58, n.3, e2021WR031508, 2022.

ASSIS, T. S. MARENGO, J. A.; AMBRIZZI, T. Land-use changes and their implications for precipitation trends in the Xingu watershed. **International Journal of Climatology**, v.43, n.2, E2022-E2037, 2023.

BARCELLOS, D. C.; NOBRE, C. A.; MARENGO, J. A. Drivers of deforestation in the Xingu watershed: An analysis of the role of agriculture and infrastructure expansion. **Environmental Research Letters**, v.16, n.6, 065005, 2021.

BARROS, F. S. M.; LIMA, J. E.; ESPINOZA, J. C. Impacts of deforestation on evapotranspiration and water availability in the Xingu watershed. **Water Resources Research**, v.58, n.2, e2021WR030569, 2022.

BARROS, F. S. M.; NOBRE, C. A.; MARENGO, J. A. Deforestation and precipitation trends in the Xingu watershed: A comprehensive assessment. **Environmental Research Letters**, v.18, n.1, 015001, 2023.

MEDEIROS, F. J.; OLIVEIRA, C. P.; AVILA-DIAZ, A. Evaluation of extreme precipitation climate indices and their projected changes for Brazil: From CMIP3 to CMIP6. **Weather and Climate Extremes**, v.38, 100511, 2022.

FEARNSIDE, P. M. Soybean cultivation as a threat to the environment in Brazil. **Environmental Conservation**, v.28, n.1,p. 23-38, 2021.

FEARNSIDE, P. M. Brazil's Cuiaba-Santarem (BR-163) highway: The environmental cost of paving a soybean corridor through the Amazon. **Environmental Management**, v.36, n.5, p.649-663, 2005.

FEARNSIDE, P. M. Deforestation in Brazilian Amazonia: history, rates, and consequences. **Conservation Biology**, v.33, n.4, p.802-809, 2019.

FONSECA, C. R.; FORZZA, R. C.; BARBOSA, M. R. V.; LIMA, J. S.; TROVÓ, M.; PEREIRA, G. A.; CARDOSO, D. Brazilian Flora 2020: Innovation and collaboration to meet Target 1 of the Global Strategy for Plant Conservation (GSPC). **Rodriguésia**, v.70, n2, e01432018, 2019.

FUNK, C.; PETERSON, P.; LANDSFELD, M.; PEDREROS, D.; VERDIN, J.; SHUKLA, S.; HUSAK, G. The climate hazards infrared precipitation with stations - a new environmental record for monitoring extremes. **Scientific Data**, v.2, 150066, 2015.

GATTI, L. V.; GLOOR, M.; MILLER, J. B. DOUGHTY, C. E.; MALHI, Y.; DOMINGUES, L. G.; BORGES, V. F. Drought sensitivity of Amazonian carbon balance revealed by atmospheric measurements. **Nature**, v.506, v.7486, p.76-80, 2018.

GILLIES, SEAN et al. **Rasterio Documentation**, 2023. Disponível em: https://rasterio.readthedocs.io/en/stable/topics/reading.html.

HOLLANDA, F. C. B.; COSTA, M. C.; MELO, M. L. D. Mercury contamination of water, soil, and plants associated with artisanal gold mining in the Xingu River Basin, Brazilian Amazon. **Environmental Monitoring and Assessment**, v.192, n.3, p.192, 2020.

HUFFMAN, G. J.; BOLVIN, D. T.; BRAITHWAITE, D.; HSU, K.; JOYCE, R.; KIDD, C.; … XIE, P. **Integrated Multi-satellitE Retrievals for GPM (IMERG) technical documentation**. Version 07. NASA/GSFC/SDSD/Rainfall Science Branch, 2021.

HUNTER, J. D. Matplotlib: A 2D Graphics Environment. Computing in **Science & Engineering**, v.9, n.3, p.90-95, 2007.

LESSA, A. R.; BARLOW, J.; FERREIRA, J.; LOUZADA, J.; PARDINI, R.; ACCACIO, G. M.; COELHO, R. Scientific support for a network of large protected areas in the Brazilian Amazon. **Perspectives in Ecology and Conservation**, v.18, n.3, p.128-133, 2020.

LUCAS, E. W. M.; SOUSA, F. D. A. S.; SANTOS SILVA, F. D.; ROCHA JÚNIOR, R. L.; PINTO, D. D. C.; SILVA, V. D. P. R. Trends in climate extreme indices assessed in the Xingu river basin-Brazilian Amazon. **Weather and Climate Extremes**, v.31, 100306, 2021.

MACHADO, F. N., et al. Linking large-scale climate patterns to hydrological changes in the Xingu River basin, eastern Amazon. **Regional Environmental Change**, v.21, n.7, p.1-14, 2021.

MARENGO, J. A.; SOUZA, L. S. P.; SOARES, W. R. South Atlantic convergence zone and its influence on precipitation patterns in the Xingu watershed. **Journal of Climate**, v.34, n.5, p.1743-1759, 2021.

MAGNONI, P. H. J., SILVA, C. D. O. F.; MANZIONE, R. L. Groundwater recharge and water table levels modelling using remotely sensed data and cloud-computing. **Sustainable Water Resources Management**, v.6, n.6, p.113, 2020.

MALHI, Y.; DOUGHTY, C. E.; GALETTI, M.; SMITH, F. A.; SVENNING, J. C.; TERBORGH, J. W. Megafauna and ecosystem function from the Pleistocene to the Anthropocene. **Proceedings of the National Academy of Sciences**, v.115, n.25, p.6241-6248, 2018.

MALHI, Y.; ROBERTS, J. T.; BETTS, R. A.; KILLEEN, T. J.; LI, W.; NOBRE, C. A. Climate change, deforestation, and the fate of the Amazon. **Science**, v.319, n.5860, p.169-172, 2018.

NEPSTAD, D.; MCGRATH, D.; ALENCAR, A.; BARROS, A. C.; CARVALHO, G.; SANTILLI, M.; VERA-DIAZ, M. C. Slowing Amazon deforestation through public policy and interventions in beef and soy supply chains. **Science**, v.344, n.6188, p.1118-1123, 2014.

MEDINA, F. D.; ZOSSI, B. S.; BOSSOLASCO, A.; ELIAS, A. G. Performance of CHIRPS dataset for monthly and annual rainfall-indices in Northern Argentina. **Atmospheric Research**, v.283, 106545, 2023.

ISSN 2318-2962
DOI 10.5752/p.2318-2962.2024v34n.78p.815

NOBRE, C. A.; BARCELLOS, D. C.; MARENGO, J. A. Deforestation and precipitation trends in the Xingu watershed: A review of recent studies. **Earth System Dynamics**, v.11, n.2, p.355-370, 2020.

NOBRE, C. A.; MALHI, Y.; COSTA, M. H.; AGUIAR, A. P. D.; VIEIRA, I. C. G.; ASSIS, T. O.; DALLA-NORA, E. L.; TOLEDO, P. M.; BATISTELLA, M. Land use change emission scenarios: anticipating a forest transition process in the Brazilian Amazon. **Global Change Biology**, v.22, n.5, p.1821-1840, 2016.

NOGUEIRA, E. M., et al. Soil-vegetation relationships in a complex landscape: the Amazonian Xingu River headwaters region. **Geoderma**, v.322, p.132-144, 2018.

OLIVEIRA, A. S., et al. Flooding regime and tree communities in the Xingu River headwaters: effects of topography, soil, and hydrology. Wetlands **Ecology and Management**, v.28, p.133-147, 2020.

PHILLIPS, O. L.; BRIENEN, R. J. W.; FELDPAUSCH, T. R. GLOOR, E. BAKER, T. R.; LLOYD, J.; ALMEIDA, S. Amazon forest dynamics and climate variability. Progress in **Physical Geography: Earth and Environment**, v.45, n.1, p.3-26, 2021.

SHEN, C.; WANG, L.; CHEN, S. Long-term precipitation trends in the Yangtze River Basin, China, based on the Mann-Kendall and Sen's slope methods. **Theoretical and Applied Climatology**, v.148, n.1-2, p.477-493, 2022.

SHRESTHA, N. K.; QAMER, F. M.; PEDREROS, D.; MURTHY, M. S. R.; WAHID, S. M.; SHRESTHA, M. Evaluating the accuracy of Climate Hazard Group (CHG) satellite rainfall estimates for precipitation based drought monitoring in Koshi basin, Nepal. **Journal of Hydrology: Regional Studies**, v.13, p.138-151, 2017.

SILVA, C. A., et al. Drought responses of floodplain trees in the lower Amazon: spatial–temporal variations and effects on forest structure. **Tree Physiology**, v.39, n.4, p.623-639, 2019.

SILVA, R. A. F.; LIMA, J. E.; ESPINOZA, J. C. Seasonal precipitation trends in the Xingu watershed: A comprehensive analysis. **International Journal of Climatology**, v.41, n.S1, E1476-E1494, 2021.

SIQUEIRA, A. D.; SCHAEFER, C. E. G. R.; SOUZA JR, V. S.; FERNANDES FILHO, E. I. The impact of mining on the vegetation of the Brazilian Amazon: a review. **Environmental Science and Pollution Research**, v.28, n.6, p.6506-6521, 2021.

TADESSE, T.; YIGZAW, W.; WONDIE, A.; BAYISSA, Y. A. Validation of Climate Hazards group InfraRed Precipitation with Station data (CHIRPS) in the Upper Blue Nile Basin. **Hydrology Research**, v.52, n.4, p.875-887, 2021.

TANG, Q.; ZHANG, X.; XIE, P. Global precipitation trends across the Northern Hemisphere during 1951-2017 based on CMIP5 models. **Climate Dynamics**, v.57, n.3-4, p.1469-1486, 2021.

ISSN 2318-2962
DOI 10.5752/p.2318-2962.2024v34n.78p.815

WU, Q.; ZUO, Q.; LI, D.; LI, J.; HAN, C.; MA, J. Integrated assessment of multiple characteristics for extreme climatic events under climate change: Application of a distribution-evolution-attribution-risk framework. **Atmospheric Research**, v.282, 106515, 2023.

ZHANG, W.; QI, J.; SUN, G. Spatiotemporal variability of precipitation and its driving factors over the Loess Plateau, China. **Journal of Hydrology**, v.585, 124811, 2020.

ZHANG, W.; QI, J.; SUN, G.; GUO, B. Spatiotemporal characteristics of precipitation and their implications for vegetation growth over the past 30 years on the Tibetan Plateau. **Journal of Arid Environments**, v.191, 104359, 2021.

Recebido: 19/06/2024
Aceito: 30/07/2024